Theory of ferroelectricity: The polarizability model

H. Bilz,* G. Benedek,† and A. Bussmann-Holder
Max-Planck-Institut für Festkörperforschung, Heisenbergstrasse 1, 7000 Stuttgart 80, Federal Republic of Germany
(Received 30 October 1986)

We consider ferroelectric compounds created by relative ionic displacements between two or more sublattices ("displacive" phase transitions). For these ferroelectric materials the nonbonding p orbitals of oxygen (O^{2-}) or chalcogen (S^{2-}, etc.) ions play a central role, which is taken into account in the dynamical theory. It turns out that the fourth-order polarizability of the chalcogen ions is the main mechanism responsible for specific dynamical properties such as phonon dispersion curves and their anomalies ("soft modes"), Raman scattering, etc. The self-consistent phonon approximation is shown to give good results at all temperatures, particularly at $T=0$ ("quantum limit") where this approximation is consistent with renormalized-group theory, and at very high temperatures ($T \gg T_c$).

I. INTRODUCTION

In a review of the lattice dynamics of ferroelectricity Gillis and Koehler[1] end their discussion with the question: "... why, for two crystals of the same lattice structure, is one ferroelectric and the other not?" They add the remark that the answer to this question is "intimately tied to a realistic description of the interatomic forces in insulators."

The present paper is mainly concerned with this problem. We are going to show that an essential part of the microscopic origin of ferroelectric phase transitions may be found in the intrinsic electronic instability of the O^{2-} ion and its homologues, S^{2-}, etc., which in ionic compounds are stabilized by long-range Coulomb forces only. This hypothesis is supported by the observation that about 99% of the known ferroelectrics are chalcogenides and 97% of them oxides.[2] We start with a short discussion of the oxygen-ion polarizability (Sec. II) and then describe a semimicroscopic vibrational model[3,4] (Sec. III) which describes the effect of the outer nonbonding p electrons of the chalcogenide ions in terms of a fourth-order electron-ion potential. This strongly localized, repulsive potential turns out to give the main part of the second-order Raman spectra in simple and in perovskitic oxides.[3] Furthermore, it leads to a quantitative understanding of the temperature dependence of soft modes in $KTaO_3$ and $SrTiO_3$.[3] In a simplified lowest-two-modes version the model is able to explain the temperature behavior of soft modes in very different systems such as SbSI (Ref. 5), K_2SeO_4 (Ref. 6), and SnTe (Ref. 7) and related compounds. Here, a self-consistent (one-loop) approximation to the interaction potential[1] is used which seems to work for second-order phase transitions as well as for (weakly) first-order cases, i.e., it fits the data nearly within the limits of experimental errors. The main result of this investigation is that simple mean-field behavior, with a value $\gamma=1$ for the critical exponent of the static susceptibility, is only an intermediate case; at very high temperatures γ tends to zero (saturation) and at very low temperatures γ approaches a value of 2 (quantum limit), except for logarithmic corrections. In this quantum regime, the upper critical dimensionality ($d=4$) becomes equal to the dimensionality of the system which is enhanced, by quantum effects, from $d=3$ to $d=4$. Therefore, the mean-field exponent of the soft-mode frequency is the critical (static) exponent of the Landau-Ginsburg-Wilson theory of a ϕ_4 model. In the high-temperature regime, on the other hand, the polarizability model exhibits a changeover from the ϕ_4 to a ϕ_2 model in marked contrast to the standard type of one-component ϕ_4 models.[8]

For the interested reader, we mention (among the numerous reviews and articles on ferroelectrics) four recent books on the subject, the first by Mitsui *et al.*,[9] providing a comprehensive introduction and survey; secondly the most useful thorough monography by Lines and Glass,[2] thirdly an investigation of photoferroelectrics by Fridkin,[10] and fourth a review on ferroelectric IV-VI compounds by Bussmann-Holder *et al.*[11]

II. THE OXYGEN POLARIZABILITY AND ITS ROLE IN FERROELECTRICS

At present, more than 450 ferroelectric and antiferroelectric substances are known (see Ref. 12 and Lines and Glass[2]) nearly all of them being chalcogenides. They may be phenomenologically divided into two classes: a first one of the "order-disorder" and a second one of the "displacive" type. This distinction is by no means as clear as it seems at the first glance: some ferroelectrics such as the KH_2PO_4 family seem to exhibit features from both types. We shall, nevertheless, use this conceptual division into two types, one built of molecular groups with *permanent* dipoles (order-disorder type), and a second one where the dipole moments are *induced* during the phase transition so that the soft-mode concept becomes important (displacive type). We are only concerned with this second type of ferroelectrics, and we shall try to understand the intrinsic relation between the formation and orientation of electric dipoles in the ferroelectric phase transition.

The rich phenomenology of ferroelectrics which differs

in many chemical and physical properties supports the opinion that several different microscopic mechanisms are responsible for the appearance of ferroelectricity in different materials. We hope to be able to demonstrate that many ferroelectrics with induced dipoles can be described by the same microscopic mechanism, i.e., the nonlinear quartic polarizability of oxygen or chalcogen ions.

The problem of the oxygen ion O^{2-} and its homologous S^{2-}, etc. can be traced back to investigations by Biltz and Klemm.[13] They found that the ionic radius of O^{2-} cannot be defined by a Goldstein rigid-ion radius. Instead space "increments" have to be introduced to describe the peculiar properties of O^{2-} in a crystal. A justification of this flexible description of the oxygen ion was phenomenologically given by Tessmann *et al.*, who investigated ionic polarizabilities as functions of different crystalline lattices.[14] While a fixed polarizability α can be ascribed to most of the investigated ions, the oxygen-ion polarizability was found to be strongly dependent on its surroundings. For instance, in simple-cubic oxides such as MgO, CaO, SrO, etc. $\alpha(O^{2-})$ depends linearly on the ionic volume. In tetrahedrally bound oxides, covalency enhances this effect to a volume-squared dependence while in spinels and ferroelectric oxides the anisotropic configuration of O^{2-} leads to $\alpha \approx V^{3-4}$.

The probability of O^{2-} has been calculated quantum mechanically within the Watson model. As O^{2-} is configurationally unstable as a free ion, Watson[16] introduced as a stabilizing potential a sphere with a uniformly charged surface to simulate the crystalline Coulomb potential. The Watson potential V_w has to fulfill the following conditions (refer to Fig. 1).

(i) The depth of the potential well is given by the Madelung potential at an oxygen lattice site and thus defines the Watson radius R_w which simultaneously is proportional to the lattice constant.

(ii) For large radii the crystalline Coulomb potential V_c is asymptotically compensated by the Watson potential V_w.

Thus wave functions and charge densities can be computed as a function of the Watson radius R_w, which are used to calculate the polarizability by means of the formalism of Thorhallson *et al.*[17]

In Fig. 2 the results of the isotropic model calculations[17] are shown. The polarizability of O^{2-} as a function of the Watson radius is compared to the polarizability of the "well-behaved" ion F^-. While in the limit $R_w \to \infty$, α of F^- converges to a constant value, the O^{2-} polarizability diverges. Within the physical relevant range of R_w, $\alpha(O^{2-})$ is proportional to R_w^3 consistent with the above-mentioned dependence of α on the cell volume phenomenologically found in simple oxides.[14]

To calculate wave functions and polarizabilities of partially covalent and anisotropic oxides one has to go beyond the Watson model. The potential is no longer spherical but should exhibit ellipsoidal features. We have simulated the effect of anisotropy within the Watson model by taking a weighted average over Watson spheres with different radii R_1, R_2.[18] The closure approximation was used and a rotational ellipsoidal polarizability assumed. This procedure led to an additional volume dependence of $\alpha(O^{2-})$ as compared to the isotropic case. Including covalency, a further enhancement should be achieved, thus eventually leading to the observed nonlinear polarizability of oxidic ferroelectric perovskites.

An interesting result about the effect of anisotropy on the O^{2-} ion has been obtained by Prat.[19] He calculated the energy levels and total energies for different configurations and symmetries using the unrestricted Hartree-Fock method. Prat found that an ellipsoidally distorted charge distribution could lead to a (meta)stable O^{2-} configuration, though the total energy of this anisotropic charge distribution is higher than that of the unstable isotropic O^{2-} configuration. Inspection of these results points to the importance of "in-out" correlations of p electron pairs with opposite spins and suggests why O^{2-} has mainly a twofold or fourfold coordination in solids as known from chemical structure data.[20]

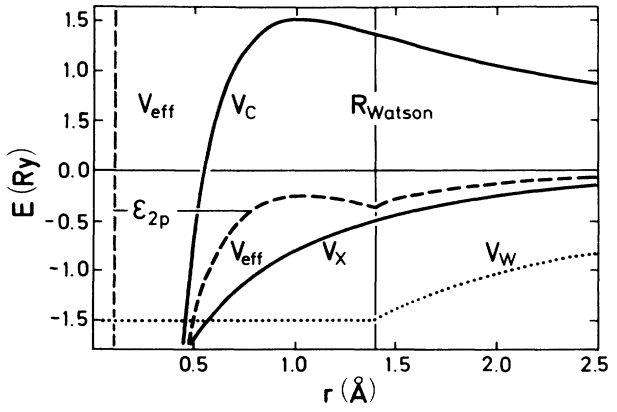

FIG. 1. The Watson sphere model for the O^{2-} ion: Coulomb potential V_c, exchange potential V_x, Watson potential V_w, resulting potential V_{eff}, and energy level of $2p$ electrons ε_{2p}.

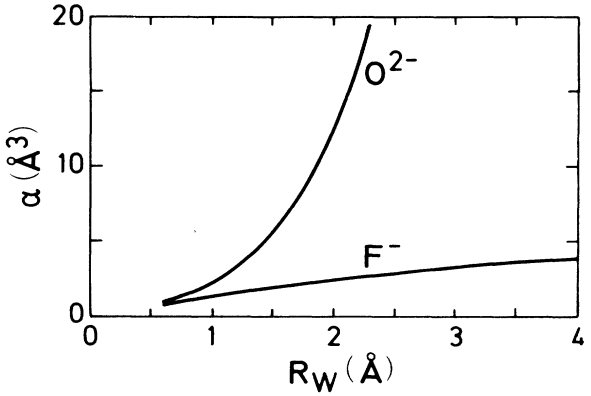

FIG. 2. Polarizabilities α of O^{2-} and F^- ions as a function of Watson radius R_w.

III. THE POLARIZABILITY MODEL

A. The three-dimensional model

The lattice dynamics of cubic perovskite (ABO_3) ferroelectrics based on a shell model was developed by Cochran and his co-workers (Ref. 21 and references therein). The inelastic neutron scattering data on $SrTiO_3$ have stimulated further detailed investigations by Cowley[22] and Stirling.[23] The shell model they used includes axially symmetric short-range forces which couple the shell of each oxygen ion to those of its nearest A, B, and O ions [refer to Fig. 3(a)]. All ions, A, B, and O, were assumed to be isotropically polarizable, each one with shell charges y_i and core-shell coupling constants K_i ($i = A$, B, O).

As discussed in the preceding section, this shell model had to be extended to take into account the nonlinear anisotropic polarizability of the oxygen O^{2-} ion. Since the oxygen-ion polarizability depends strongly on its crystalline environment, two independent core-shell force constants were considered for this ion: K_{OB} for shell core displacements directed towards its neighboring B ions and K_{OA} for those lying in the plane where the oxygen is surrounded by four A neighbors [Fig. 3(b)]. This model was developed by Migoni, Bilz, and Bäuerle,[3] who successfully calculated the soft modes of $SrTiO_3$ and $KTaO_3$. In their model the lowest term of the nonlinear core-shell interaction at the oxygen-ion site is of fourth order because of inversion symmetry in the paraelectric phase. It includes four independent parameters $K_{OB,B}$, $K_{OB,A}$, $K_{OA,B}$, and $K_{OA,A}$ where each A or B corresponds to a pair of core-shell displacements, as a consequence of the oxygen site symmetry. However, it has been shown[3,24] that the temperature dependence of the soft mode and other low-frequency modes as well as the Raman spectra depend on $K_{OB,B}$ only.[25] This corresponds to the modulation of the oxygen-ion polarizability in the direction of the neighboring transition-metal ions (Ti,Ta) and indicates that the phonon-induced change of the transition-metal–oxygen bond, i.e., the hybridization of oxygen p and transition-metal d electrons, plays an essential role for the dynamical properties of ferroelectrics ("dynamical covalency," refer to Bilz *et al.*[26]).

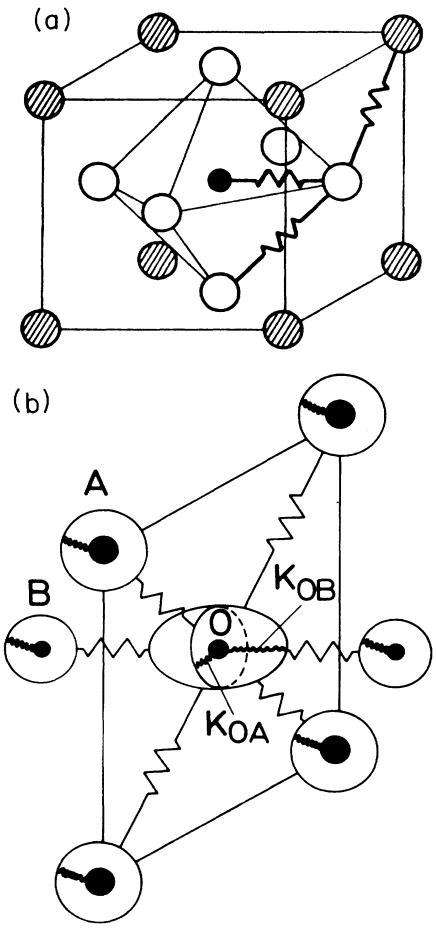

FIG. 3. (a) The perovskite (ABO_3) structure. Slashed circles represent the A sublattice, open circles the oxygen ions, and solid circles the B sublattice ions, respectively. (b) Location of oxygen ions in the perovskite structure. The ellipsoid at the oxygen-ion site represents the symmetry of its polarizability. The springs within the ellipsoid refer to the anisotropic core-shell couplings. The shells of A and B ions are isotropically coupled to the respective cores.

The importance of the p-d hybridization represented by $K_{OB}(T)$ has recently been demonstrated for the mixed crystals of $KTa_{1-x}Nb_xO_3$.[27] The hyper-Raman data on these compounds[28] have been interpreted on the basis of the above-described model. It was shown that the temperature dependence of the soft modes as a function of composition x is only due to the effective core-shell coupling $K_{OB}(T)$.[29] On the basis of these previous analyses it becomes clear that the relevant dynamical and critical features of perovskites and other ferroelectrics are controlled by a limited number of parameters, much less than required in a three-dimensional treatment. A physically more transparent form can be achieved by considering only the crystalline ferroelectric axis as the lattice dynamical relevant one.

The technical procedure for this reduction is simple and straightforward and can be exemplified for a perovskite structure[4] without loss of generality. In a first step of this procedure the BO_3 unit is lumped together to one large highly polarizable mass m_1. The intracluster forces K_{OB} and $K_{OB,B}$ are replaced by local core-shell couplings g_2 and g_4, where g_2 also includes the attractive Coulomb forces which destabilize the ferroelectric mode. This means that g_2, unlike K_{OB}, is a negative quantity. Stabilization is achieved via the fourth-order attractive core-shell interaction g_4, which plays exactly the same role as $K_{OB,B}$. In the next step the three-dimensional "pseudo-NaCl" structure is projected onto the ferroelectric [100] direction. The three-dimensional character, important for the calculation of critical properties, is, nevertheless, maintained in the phase-space integrations.

B. Layer model of cubic and uniaxial ferroelectrics

The Hamiltonian of the model reads

$$H = T + V \ ,$$

where

$$T=\tfrac{1}{2}\sum_n (m_1\dot{u}_{1n}^2+m_2\dot{u}_{2n}^2+m_{e1}\dot{v}_{1n}^2+m_{e2}\dot{v}_{2n}^2)\ , \quad (1)$$

$$\begin{aligned}V=\tfrac{1}{2}\sum_n [&f_1'(u_{1n}-u_{1n-1})^2+f_2'(u_{2n}-u_{2n-1})^2\\&+f(v_{2n}-v_{1n})^2+f(v_{2n}-v_{1n+1})^2\\&+g_2^{(1)}(v_{1n}-u_{1n})^2+g_2^{(2)}(v_{2n}-u_{2n})^2\\&+\tfrac{1}{2}g_4(v_{1n}-u_{1n})^4]\ ,\end{aligned} \quad (2)$$

and m_1, m_{e1}, m_2, and m_{e2} are the core and shell masses of atoms 1 and 2, respectively; u_{1n}, v_{1n}, u_{2n}, and v_{2n} are their displacements in the nth cell; f, f_i', and $g_2^{(i)}$ $(i=1,2)$ are shell-shell, core-core, and internal shell-core harmonic force constants (Fig. 4) while the anharmonic constant g_4 accounts for the nonlinear polarizability of atom 1. In general, only one of the two ionic species of the diatomic lattice exhibits a strongly nonlinear temperature-dependent polarizability. From the definition

$$w_{in}=v_{in}-u_{in}\quad (i=1,2) \quad (3)$$

we have

$$\begin{aligned}V=\tfrac{1}{2}\sum_n [&f_1'(u_{1n}-u_{1n-1})^2+f_2'(u_{2n}-u_{2n-1})^2\\&+f(u_{2n}-u_{1n}+w_{2n}-w_{1n})^2\\&+f(u_{2n}-u_{1n+1}+w_{2n}-w_{1n+1})^2\\&+g_2^{(1)}w_{1n}^2+g_2^{(2)}w_{2n}^2+\tfrac{1}{2}g_4w_{1n}^4]\ .\end{aligned} \quad (4)$$

Taking into account the adiabatic conditions

$$\frac{\delta V}{\delta v_{1n}}=0\ , \quad (5)$$

$$\frac{\delta V}{\delta v_{2n}}=0\ , \quad (6)$$

we write the equations of motion as follows:

$$\begin{aligned}m_1\ddot{u}_{1n}=&f(u_{2n}+u_{2n-1}-2u_{1n}+w_{2n}+w_{2n-1}-2w_{1n})\\&+f_1'(u_{1n+1}+u_{1n-1}-2u_{1n})\ ,\end{aligned} \quad (7)$$

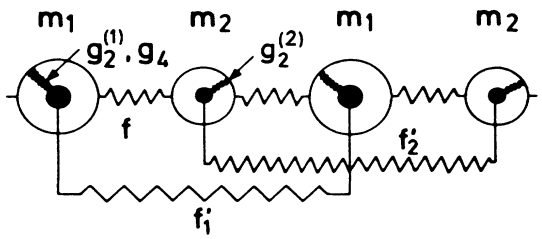

FIG. 4. Layer model of cubic and uniaxial ferroelectrics.

$$\begin{aligned}m_2\ddot{u}_{2n}=&f(u_{1n}+u_{1n+1}-2u_{2n}+w_{1n}+w_{1n+1}-2w_{2n})\\&+f_2'(u_{2n+1}+u_{2n-1}-2u_{2n})\ ,\end{aligned} \quad (8)$$

$$\begin{aligned}0=&(2f+g_2^{(1)})w_{1n}+g_4w_{1n}^3\\&-f(u_{2n}+u_{2n-1}-2u_{1n}+w_{2n}+w_{2n-1})\ ,\end{aligned} \quad (9)$$

$$\begin{aligned}0=&(2f+g_2^{(2)})w_{2n}\\&-f(u_{1n}+u_{1n+1}-2u_{2n}+w_{1n}+w_{1n+1})\ .\end{aligned} \quad (10)$$

Here we discuss the approximate solutions in the self-consistent phonon approximation (SPA) in order to analyze explicitly the temperature dependence of soft modes and related quantities. It is important to mention that this model admits exact nonlinear solutions in the form of traveling waves which have been treated in a separate paper.[30]

C. Self-consistent phonon approximation (SPA)

The SPA for Eqs. (7)–(10) corresponds to a linearization of the cubic term in the displacement coordinate w_{1n}, i.e.,

$$g_4(w_{1n})^3\simeq 3g_4w_{1n}\langle(w_{1n})^2\rangle_T\equiv g_T^{(1)}w_{1n}\ , \quad (11)$$

where

$$\langle(w_{1n})^2\rangle_T=\sum_{\mathbf{q}j}\frac{\hbar}{2N\omega_{\mathbf{q}j}}w_1^2(\mathbf{q}j)\coth\left[\frac{\hbar\omega_{\mathbf{q}j}}{2k_BT}\right]\ . \quad (12)$$

The dynamical information enters (12) through the SPA eigenvalues $\omega_{\mathbf{q}j}$ and related eigenvectors $w_1(\mathbf{q}j)$ for all phonon branches j and all wave vectors $\mathbf{q}$ in the first Brillouin zone. Taking this average in the equations of motion is of course not equivalent to a similar average in the free energy. We shall discuss this point in a later subsection, and proceed for the moment to a direct solution of the equations of motion. We shall see that this procedure is very close to the rigorous one. In this approximation Eq. (9) now reads

$$\begin{aligned}(2f+g^{(1)})w_{1n}=&f(u_{2n}+u_{2n-1}-2u_{1n}\\&+w_{2n}+w_{2n-1})\ ,\end{aligned} \quad (13)$$

where

$$g^{(1)}=g_2^{(1)}+g_T^{(1)},\quad g^{(2)}\equiv g_2^{(2)}\ . \quad (14)$$

In the paraelectric regime $(T>T_c)$, $g^{(1)}$ is positive and changes sign at the transition temperature T_c. At the transition temperature,

$$\langle w_{1n}^2\rangle_{T_c}=-g_2^{(1)}/3g_4\equiv w_0^2/3\ , \quad (15)$$

where $w_0^2=-g_2^{(1)}/g_4$ means the relative shell-core displacement at the potential minima. With this condition, we now obtain stable solutions from the equations of motion. Using standard Fourier transform, we obtain the following equations in q space:

$$\omega^2\begin{vmatrix}m_1&0\\0&m_2\end{vmatrix}\begin{vmatrix}U_1\\U_2\end{vmatrix}=D(q)\begin{vmatrix}U_1\\U_2\end{vmatrix}\ , \quad (16)$$

with a force-constant matrix

$$D(q)=2\tilde{f}\begin{vmatrix}1+A_1\sin^2(aq) & -\cos(aq)\\ -\cos(aq) & 1+A_2\sin^2(aq)\end{vmatrix} . \quad (17)$$

We have defined the T- and q-dependent effective force constant

$$\tilde{f}\equiv\frac{f}{1+2f/g_r+(4f^2/g^{(1)}g^{(2)})\sin^2(aq)} \quad (18)$$

with

$$g_r=g^{(1)}g^{(2)}/(g^{(1)}+g^{(2)}) , \quad (19)$$

$$A_1=\frac{2f_1'}{\tilde{f}}+\frac{2f}{g^{(2)}},\quad A_2=\frac{2f_2'}{\tilde{f}}+\frac{2f}{g^{(1)}} . \quad (20)$$

The shell-core eigenvectors W_1 and W_2 are related to the eigenvectors U_1 and U_2 by the equations

$$W_1=\frac{2\tilde{f}}{g^{(1)}}\left[U_2\cos(aq)-\left[1+\frac{2f}{g^{(2)}}\sin^2(aq)\right]U_1\right] , \quad (21)$$

$$W_2=\frac{2\tilde{f}}{g^{(2)}}\left[U_1\cos(aq)-\left[1+\frac{2f}{g^{(1)}}\sin^2(aq)\right]U_2\right] . \quad (22)$$

The dispersion relation can be written explicitly as

$$\omega_\pm^2(q)=\tilde{f}\left\{\frac{1}{m_1}[1+A_1\sin^2(aq)]+\frac{1}{m_2}[1+A_2\sin^2(aq)]\right.$$
$$\pm\left[\left[\frac{1}{m_1}[1+A_1\sin^2(aq)]-\frac{1}{m_2}[1+A_2\sin^2(aq)]\right]^2+\frac{4\cos^2(aq)}{m_1m_2}\right]^{1/2}\Bigg\} . \quad (23)$$

Figure 5 shows the fitting of these dispersion curves to the experimental data of $KTaO_3$.[31] The model parameters are

$$m_1=2.88\times10^{-22}\text{ g},\quad m_2=0.649\times10^{-22}\text{ g} ,$$
$$f=4.067\times10^4\text{ gs}^{-2},\quad f_1'=0.581\times10^4\text{ gs}^{-2} ,$$
$$g_2^{(1)}=-0.828\times10^4\text{ gs}^{-2} ,$$
$$g_4=0.255\times10^{22}\text{ gs}^{-2}\text{cm}^{-2}\quad (f_2'=g_2^{(2)}=0) .$$

In the limit $q\to0$ the acoustic mode dispersion is

$$\omega_-^2(q)\simeq\frac{2}{m_1m_2}(f+2f_1'+2f_2')\sin^2(aq) , \quad (24)$$

while the ferroelectric mode tends to

$$\omega_+^2(0)\equiv\omega_F^2=\frac{2f}{\mu}\frac{1}{1+2f/g_r}$$
$$\equiv\omega_0^2/(1+2f/g_r) . \quad (25)$$

Here, μ is the reduced cell mass and ω_0^2 is the rigid-ion limit of ω_F^2, when both $g^{(i)}\to\infty$.

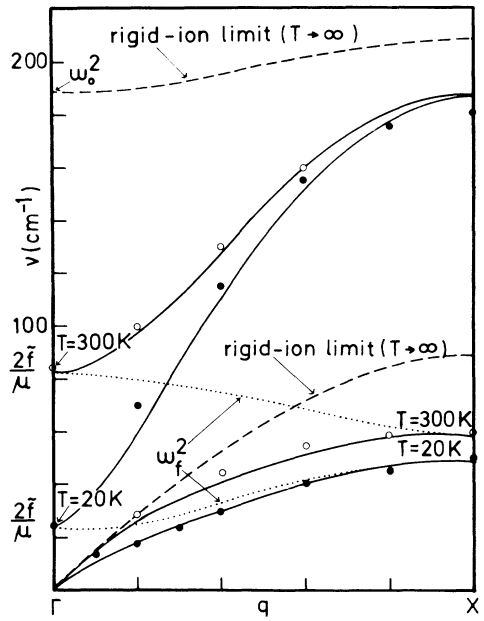

FIG. 5. Comparison of theoretical (solid lines) and experimental (Ref. 31) (dots) dispersion curves for $T=20$ K (solid dots) and $T=300$ K (open dots) for $KTaO_3$. Dotted lines represent the temperature and q-dependent interpolated ferroelectric mode [Eq. (31)], while dashed lines reproduce the rigid-ion limit, i.e., $g^{(1)}\to\infty$.

At the zone boundary ($aq=\pi/2$) we have

$$\omega_+^2\left[\frac{\pi}{2a}\right]=\frac{2}{m_2}\left[\frac{f}{1+2f/g^{(2)}}+2f_2'\right] , \quad (26)$$

$$\omega_-^2\left[\frac{\pi}{2a}\right]=\frac{2}{m_1}\left[\frac{f}{1+2f/g^{(1)}}+2f_1'\right] . \quad (27)$$

It is important to remark that the limits $q\to0$ and $g_r\to0$ cannot be interchanged. At the phase transition ($g_r=0$, $\omega_F^2=0$) the ferroelectric branch degenerates into a pseudoacoustic branch, since our system splits now into two independent chains. Thus, for $g^{(1)}=0$ and small q

$$\omega_+^2(q)\simeq[(2f+4f_2')/m_2]\sin^2(aq) , \quad (28)$$

$$\omega_-^2(q)\simeq(4f_1'/m_1)\sin^2(aq) \quad (29)$$

D. Temperature dependence and critical regimes

We now proceed to a calculation of the thermal averages of $\langle w_{1n}^2\rangle_T$ [Eq. (12)] by means of Eqs. (21) and (22). Since $\langle w_{1n}^2\rangle_T$ is a function of ω_F^2 and T we obtain from Eqs. (11), (12), and (25) a single self-consistent equation giving the implicit relation between ω_F^2 and T,

$$g_2^{(1)}(1-\omega_F^2/\omega_0^2)+3g_4(1-\omega_F^2/\omega_0^2)^3I_F(\omega_F,T)=\mu\omega_F^2 , \quad (30)$$

where I_F is an integral over the three-dimensional Brillouin zone containing all the dynamical information.

Here we want to discuss the analytical behavior of ω_F for various temperature regimes. To this purpose we use in the calculation of $\langle w_{1n}^2 \rangle_T$ only what is analytically relevant, that is the ferroelectric branch with some simplifying assumption, i.e., $g^{(2)}=\infty$ and an isotropic dispersion with a Debye-like behavior at large q:

$$\omega_f^2(q) \sim \omega_F^2 + (4f_1'/m_1)a^2q^2 . \tag{31}$$

This dispersion relation connects the zone-center ferroelectric mode to the T-dependent zone-boundary mode. For $m_1 > m_2$ the latter is the acoustic mode, and therefore Eq. (31) neglects the noncrossing between optical and acoustic modes. In the opposite case ($m_1 < m_2$), Eq. (31) just describes the T-dependent optical branch. For this branch [Eq. (31)] we have in all cases a relationship between the core eigenvectors

$$m_2 U_2 = -m_1 U_1 \cos(aq) \tag{32}$$

with the normalization condition

$$m_1 U_1^2 + m_2 U_2^2 = 1 . \tag{33}$$

By inserting Eqs. (32) and (33) in Eq. (21) and using the approximation $g^{(2)} \to \infty$ [all apices (1) are dropped], we have

$$W_1^2(q) = \frac{1}{m_1}\left[\frac{2\tilde{f}}{g}\right]^2 \left[1+\frac{m_1}{m_2}\cos^2(aq)\right] . \tag{34}$$

Consistently with a Debye behavior, the integral can be rewritten as

$$I_F(\omega_F,T) \approx \frac{3\hbar}{2\mu\omega_D^3} \int_0^{\omega_D} \frac{\omega^3}{(\omega_F^2+\omega^2)^{1/2}} \times \coth\left[\frac{\hbar(\omega_F^2+\omega^2)^{1/2}}{2k_BT}\right] d\omega , \tag{35}$$

where $\omega_D \equiv (f_D/\mu)^{1/2}$ is a Debye frequency and f_D is the related force constant. The reduced mass μ is used instead of m_1 in order to account for the temperature-independent branch neglected in the integration. This is enough to ensure completeness, and therefore to give a correct description of ω_f^2 also in the high-temperature limit. The analytical behavior of I_F determines the T dependence of ω_F^2 in different regimes.

E. High-temperature regime ($2k_BT > \hbar\omega_D$)

For large T, i.e., $2k_BT > \hbar\omega_D$, the hyperbolic cotangent can be replaced by the reciprocal of its argument, which gives

$$I_F(\omega_F,T) \simeq \frac{3k_BT}{\mu\omega_D^2}\left[1-\frac{\omega_F}{\omega_D}\arctan\left[\frac{\omega_D}{\omega_F}\right]\right] , \tag{36}$$

and when $\omega_F \ll \omega_D$ the arctan term drops out, the *mean-field* relation,

$$\omega_F^2 = \frac{|g_2|}{\mu T_c}(T-T_c) \quad (T \geqq T_c) , \tag{37}$$

is obtained, where

$$k_BT_c = \frac{f_D|g_2|}{9g_4}, \quad 2k_BT_c > \hbar\omega_D \tag{38}$$

is mass independent. It is interesting to note that the expression for T_c in the classical limit can be worked out exactly for our model restricting to the simplified assumption made in Eq. (31). The expression of T_c involves an integral over *both* acoustic and optical branches:

$$k_BT_c = \frac{|g_2|}{9g_4}\frac{1}{V_c/3\int dq q^2[(1/f)\cot^2(aq)+(1/2f_1')\csc^2(aq)]} \tag{39}$$

where V_c is the cell volume. The integral in the denominator defines the inverse of an effective force constant, which, according to Eq. (38), is just f_D. For increasing T, ω_F^2 deviates from linearity and tends to the rigid-ion value (saturation) according to the asymptotic expression

$$\omega_F^2 \sim \omega_0^2[1-(f_D^2/3g_4k_BT)^{1/3}] . \tag{40}$$

When the mass m_1 refers to a polarizable cluster, e.g., the BO_3 units in ABO_3 perovskites, the shell mass m_{e1} cannot be neglected anymore. This nonadiabatic treatment changes the asymptotic critical exponent from $\frac{1}{3}$ to approximately $\frac{1}{2}$, which also has been verified experimentally.[32,33,29]

The behavior of ω_F near the phase transition ($T=T_c$, $\omega_F=0$) can be derived analytically for the quantum ($2k_BT_c < \hbar\omega_D$) as well as the classical mean-field regimes ($2k_BT_c \geqq \hbar\omega_D$) by making use of the approximations for the hyperbolic cotangent

$$\coth x = \begin{cases} 1/x, & x \leqq 1 \\ 1, & x > 1 \end{cases} \tag{41}$$

therefore for small ω_F, i.e., $\omega_F \ll \omega_D$, we distinguish the following cases

(i) $(2k/\hbar)T \geqq \omega_D \gg \omega_F$ (classical ferroelectric, e.g., SbSI),

$$I_F \simeq \frac{3k_BT}{f_D}\left[1-\frac{\pi}{2}\frac{\omega_F}{\omega_D}+\left[\frac{\omega_F}{\omega_D}\right]^2\right] . \tag{42a}$$

(ii) $\omega_D \gg (2k/\hbar)T > \omega_F$ (quantum ferroelectric, e.g., $KTaO_3$),

$$I_F \simeq \frac{3\hbar\omega_D}{4f_D}\left\{1+\left[\frac{2k_BT}{\hbar\omega_F}\right]^2-\pi\frac{2k_BT}{\hbar\omega_D}\frac{\omega_F}{\omega_D}+\left[\frac{\omega_F}{\omega_D}\right]^2\left[1+\ln\left[\frac{2k_BT}{\hbar\omega_D}\right]\right]\right\}. \quad (42b)$$

(iii) $\omega_D \gg \omega_F > (2k/\hbar)T$ (incipient ferroelectric, e.g., PbTe),

$$I_F \simeq \frac{3\hbar\omega_D}{4f}\left\{1+\left[\frac{\omega_F}{\omega_D}\right]^2\left[\tfrac{1}{2}+\ln\left[\frac{\omega_F}{2\omega_D}\right]\right]\right\}. \quad (42c)$$

It has to be pointed out that no T dependence is left in the expansion for the incident ferroelectric case, Eq. (42c). By differentiating Eq. (30) and using the expansions (42a) and (42b), we find

$$\frac{dT}{d\omega_F}=\frac{F_c\omega_F+\pi T}{2\omega_D-\pi\omega_F} \quad \text{(classical ferroelectric)}, \quad (43a)$$

$$\frac{dT}{d\omega_F}=\frac{F_q\omega_F+\pi T-(\hbar\omega_F/k_B)\ln(2k_BT/\hbar\omega_D)}{4k_BT/\hbar-\pi\omega_F} \quad \text{(quantum ferroelectric)}, \quad (43b)$$

where

$$F_c=\frac{4T_c}{\omega_D}(2\rho-1), \quad (44a)$$

$$F_q=\frac{2\hbar}{k_B}\left\{\left[1+\left[\frac{2k_BT_c}{\hbar\omega_D}\right]^2\right]\rho-1\right\}, \quad (44b)$$

and

$$\rho=\left[1-\frac{f}{g_2}\right]\frac{f_D}{f}. \quad (45)$$

The respective transition temperatures are given by Eq. (38) or (39) for the classical regime, and by

$$k_BT_c \sim -\tfrac{1}{2}\hbar\left[\frac{f_D}{\mu}\right]^{1/2}\Big/\ln\left[\frac{\mu}{\mu_c}-1\right] \quad (46)$$

for the quantum regime. The quantum limit ($T_c \to 0$) occurs when μ approaches from above the critical reduced-mass value

$$\mu_c=\frac{1}{f_D}\left[\frac{9\hbar g_4}{4g_2}\right]^2. \quad (47)$$

In this limit the zero-point fluctuations are

$$\langle w_1^2\rangle_{T=0}=\frac{3}{4}\frac{\hbar}{\mu\omega_D}. \quad (48)$$

If $\mu < \mu_c$, we have the incipient ferroelectric case with an imaginary T_c.

By inspection of Eq. (43) we see that, for any finite T_c, ω_F^2 grows proportionally to $T-T_c$ if ω_F is greater than $\pi T_c/F_{c,q}$ [but still smaller than $2T$ for the expansions (42) to be valid].

According to the mean-field behavior, but for $\omega_F \leqq T_c/F_{c,q}$, the critical exponent becomes larger than 1 and is 2 at $\omega_F=0$. In most cases $F_{c,q} \gg 1$, so that such deviation occurs only at small ω_F and is not observed. Figure 6(a) shows a calculation of ω_F^2 and of $\langle\omega_1^2\rangle$ as functions of T for $KTaO_3$ as derived from the fitting mentioned above (Fig. 5). Deviations from the mean-field behavior (dotted line) occur in the quantum regime and at high temperature due to saturation. However, the crossover between the quantum and the mean-field regimes is much more evident in the logarithmic plot of Fig. 6(b). A

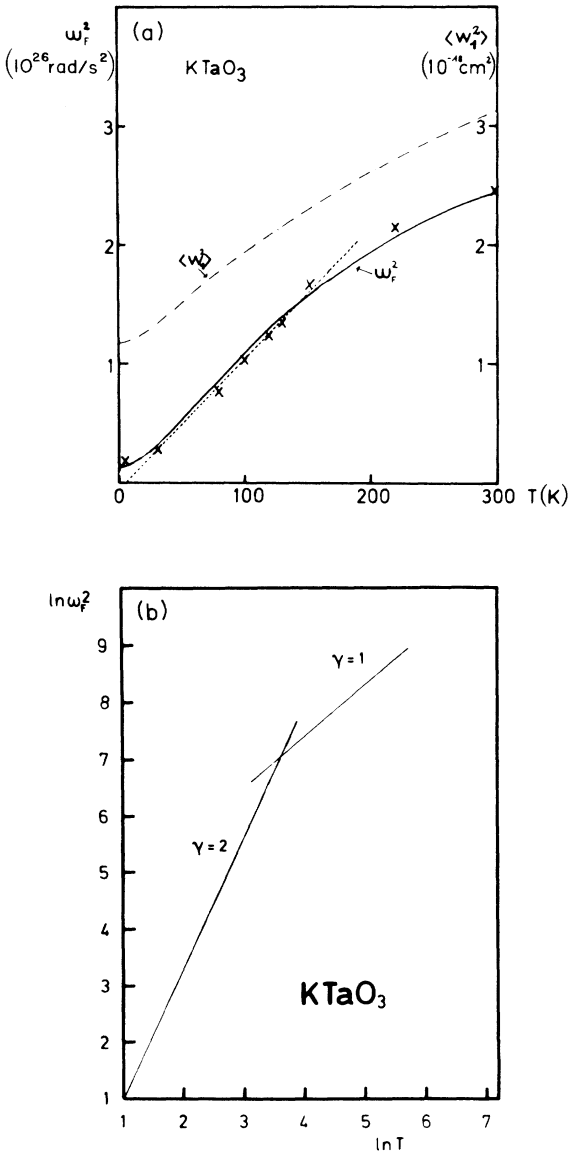

FIG. 6. (a) Calculated temperature dependence of ω_F^2 (solid line) and $\langle w_1^2\rangle$ (dashed line) for $KTaO_3$. The mean-field regime is indicated by the dotted line. Experimental data (crosses) have been taken from Ref. 31. (b) Double logarithmic plot of ω_F^2 as a function of temperature for $KTaO_3$.

systematic analysis of other ferroelectric materials whose T-dependent phonon data are accessible will be given in a subsequent paper.

F. Comparison with renormalization-group theory

In the quantum limit ($T_c=0$), T and ω_F go to zero simultaneously. One can easily prove that the logarithmic term in (43b) is the leading one that ω_F has to vanish faster than T. This yields the quantum behavior $\omega_F^2 \sim T^2$ with a logarithmic correction. More precisely,

$$\omega_F^2 \sim 8\omega_D^2 \left| \mathrm{Ei}\left[2\ln\left[\frac{k_B T}{\hbar\omega_D} \right] \right] \right|$$

$$\sim 8(k_B T/\hbar)^2 / \ln(\hbar\omega_D / k_B T) \ , \tag{49}$$

where Ei is the exponential integral.

The presence of a logarithmic correction is consistent with the result of renormalization-group theory for the number of field components going to infinity. The renormalization-group theory predicts in the quantum limit[34]

$$\omega_F^2 \sim |\ln T^2|^{-1+\delta} \ , \tag{50}$$

where $\delta \equiv 6/(n+8)$ and n is the number of field components. By expanding (50) with respect to δ

$$\omega_F^2 \sim |\ln T^2|^{-1}(1+\delta \ln|\ln T^2| + \cdots) \ , \tag{51}$$

we note that the leading term is the first one when

$$\delta \ll \ln^{-1}|\ln T^2| \ , \tag{52}$$

namely

$$T \gg \Theta_0 \exp\left[-\exp\left[\frac{n+8}{6} \right] \right] \equiv T_Q \tag{53}$$

with

$$\Theta_0 \equiv \frac{\hbar\omega_D}{k_B} \ .$$

T_Q represents the temperature above which the self-consistent quantum approximation holds (i.e., the logarithmic corrections are approximation holds (i.e., the logarithmic corrections are approximately the same for *all* n), and below which critical fluctuations take place and mean-field approximation breaks down. For $n=1$, $T_Q=0.11\Theta_0$ and for $n=3$, $T_Q=0.0019\Theta_0$. Above T_Q the logarithmic correction has always exponent -1 as our three-dimensional SPA correctly predicts. For $T<T_Q$ the logarithmic exponent tends to the exponent appropriate to the number of components n. For $n=3$, e.g., the exponent is $-\frac{5}{11}$. However, the domain where critical fluctuations take place is very small compared to the Debye temperature, and tends to zero as $n\to\infty$. For this reason we believe that it would be very difficult to check the logarithmic correction in the extreme quantum limit. Figure 7 shows the expected behavior of $\ln(\omega_F^2/T^2)$ versus $\ln|\ln T^2|$ for the cases discussed above.

G. Transition temperature and isotope effect

It is useful to have at hand a quantitative picture of how the transition temperature depends on the model parameters such as the ionic masses and the shell-core linear and nonlinear force constants (while keeping $g_2^{(2)}=\infty$ and $g_2^{(1)}=g_2$). Let us reconsider Eq. (30) at the transition temperature ($T=T_c$, $\omega_F=0$):

$$g_2 = -3g_4 I_F(0,T_c)$$

$$= -\frac{9\hbar g_4}{4\mu\omega_D}\mathcal{F}\left[\frac{\hbar\omega_D}{2k_B T_c} \right] \ , \tag{54}$$

where

$$\mathcal{F}(y) \equiv 2y^{-2}\int_0^y dx\, x\coth x \tag{55}$$

is a monotonous function with the limits $\mathcal{F}(\infty)=1$ and $\mathcal{F}(y)\sim 2/y$ for $y\to 0$. For an explicit form of T_c we can approximate $\mathcal{F}(y)$ as

$$\mathcal{F}(y) \simeq \coth(y/2) \tag{56}$$

which permits solution with respect to T_c:

$$k_B T_c = \frac{\hbar(f_D/\mu)^{1/2}}{4\,\mathrm{arcoth}(\mu^{1/2}/\mu_c^{1/2})} \ . \tag{57}$$

A plot of T_c as a function of the reduced mass μ is shown in Fig. 8. The saturation of T_c for large μ, i.e., the mass

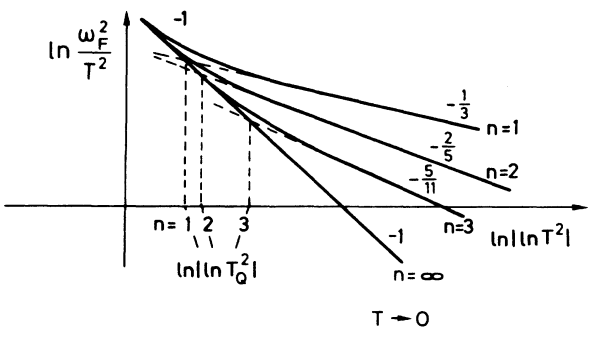

FIG. 7. Double logarithmic plot of ω_F^2/T^2 as function of $|\ln T^2|$.

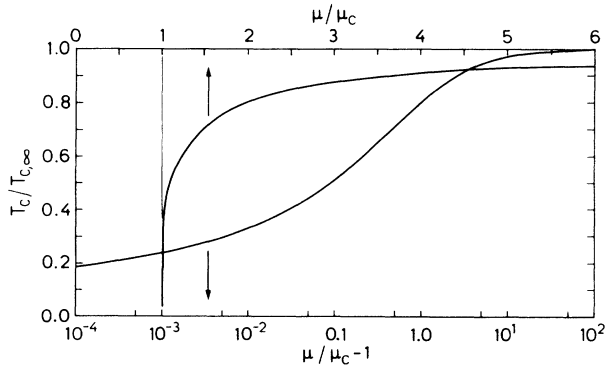

FIG. 8. The critical temperature ratio $T_c/T_{c,\infty}$ as a function of the reduced-mass ratio μ/μ_c.

independence in the classical limit, is evident. On the other hand, T_c goes very rapidly to zero as the reduced mass approaches from above the critical value $\mu_c=(9\hbar g_4/4g_2)^2/f_D$. In other words, the isotope effect on the transition temperature is larger and larger in the quantum limit and vanishes, as expected, in the high-T_c classical limit. In the quantum limit the mass dependence of T_c exhibits the logarithmic behavior given by Eq. (46).

H. Ferroelectric regime

In this paragraph we derive the dynamical parameter for the ferroelectric phase ($T<T_c$). We start from the expression of the free energy as a sum of contributions coming from the rigid-ion potential energy V_0, the potential energy V due to the static shell-core displacement $\langle w_1^2\rangle_T$, and the temperature-dependent dynamical part due to SPA phonons,

$$F=V_0+V+k_BT\sum_q \ln\left[2\sinh\left[\frac{\hbar\omega_f(q)}{2k_BT}\right]\right], \tag{58}$$

$$V=\tfrac{1}{2}g_2\langle w_1\rangle_T^2+\tfrac{1}{4}g_4\langle w_1\rangle_T^4 , \tag{59}$$

where once more the sum is restricted to the ferroelectric branch and we set $g^{(2)}=\infty$. The equilibrium configuration is given by

$$0=\frac{\partial F}{\partial\langle w_1\rangle}=\langle w_1\rangle_T(g_2+g_4\langle w_1\rangle_T^2)+\frac{1}{2N}\sum_q\frac{\hbar}{2\omega_f(q)}\frac{\partial\omega_f^2(q)}{\partial\langle w_1\rangle_T}\coth\left[\frac{\hbar\omega_f(q)}{2k_BT}\right], \tag{60}$$

where $\omega_f(q)$ is given by (31). By writing

$$\frac{\partial\omega_f(q)}{\partial\langle w_1\rangle_T}=2\langle w_1\rangle_T\frac{\partial g}{\partial\langle w_1\rangle_T^2}\frac{\partial\omega_f^2(q)}{\partial g} , \tag{61}$$

we have from (18) and (34)

$$\frac{\partial\omega_f^2(q)}{\partial g}=\frac{\partial\tilde{f}}{\partial g}\left[\frac{2}{\mu}-\frac{2}{m_2}\sin^2qa\right]=\frac{1}{m_1}\left[\frac{2\tilde{f}}{g}\right]\left[1+\frac{m_1}{m_2}\cos^2(qa)\right]=w_1^2(q) . \tag{62}$$

With $\partial g/\partial\langle w_1\rangle^2=3g_4$, we find that the driving force

$$\frac{\partial F}{\partial\langle w_1\rangle_T}=\langle w_1\rangle_T(g_2+g_4\langle w_1\rangle_T^2+3g_4\langle w_1^2\rangle_T) \tag{63}$$

is vanishing for either $\langle w_1\rangle=0$ (paraelectric phase) or

$$\langle w_1\rangle_T=\pm\left[\frac{g_2}{g_4}-3\langle w_1^2\rangle_T\right]^{1/2}=\pm[2(\langle w_1^2\rangle_{T_c}-\langle w_1^2\rangle_T)]^{1/2} , \tag{64}$$

in the *ferroelectric* phase. Since

$$\frac{\partial^2V}{\partial\langle w_1\rangle_T^2}=g_2+3g_4\langle w_1\rangle_T^2 , \tag{65}$$

we can write the shell-core force constant in the ferroelectric phase as

$$g_{\rm FE}=g_2+3g_4\langle w_1\rangle_T^2+3g_4\langle w_1^2\rangle_T=-2g_2-6g_4\langle w_1^2\rangle_T=-2g_{\rm PE} . \tag{66}$$

As a consequence, the slope of ω_F^2, when vanishing for $T\to T_c$, is steeper on the ferroelectric (FE) side as compared with the paraelectric (PE) side.

IV. SUMMARY

The model described above based on the local nonlinear chalcogenide ion polarizability provides a comprehensive description of displacive-type ferroelectric phase transitions. Within the self-consistent-phonon approximation different temperature ranges of the ferroelectric soft mode, i.e., quantum regime, classical mean-field behavior, and saturation regime, have been obtained and found to coincide with the experimentally observed phenomena. Furthermore, the model predicts logarithmic corrections in the quantum limit consistent with the results of the renormalization-group theory. In this paper we have presented, as an example, an application of the theory to $KTaO_3$. A systematic analysis of further ferroelectric materials will be given in a subsequent paper.

ACKNOWLEDGMENTS

The authors are gratefully indebted to H. Thomas for stimulating discussions and to H. Vogt for critically reading the manuscript. One of us (G.B.) acknowledges the hospitality of the Max-Planck-Institut FKF, Stuttgart, where this work was completed.

*Deceased.
†Dipartimento di Fisica dell'Universitá and Gruppo Nazionale di Struttura della Materia del Consiglio Nazionale delle Ricerche, Via Celoria 16, 20133 Milano, Italy.

[1]N. S. Gillis and T. R. Koehler, Phys. Rev. B **5**, 1924 (1972).
[2]M. E. Lines and A. M. Glass, *Principles and Applications of Ferroelectrics and Related Materials* (Clarendon, Oxford, 1977).
[3]R. Migoni, H. Bilz, and D. Bäuerle, Phys. Rev. Lett. **37**, 1155 (1976).
[4]H. Bilz, A. Bussmann, G. Benedek, H. Büttner, and D. Strauch, Ferroelectrics **25**, 339 (1980).
[5]M. Balkanski, M. K. Teng, M. Massot, and H. Bilz, Ferroelectrics **26**, 737 (1980).
[6]H. Bilz, H. Büttner, A. Bussmann-Holder, W. Kress, and U. Schröder, Phys. Rev. Lett. **48**, 264 (1982).

[7]A. Bussmann-Holder, H. Bilz, and W. Kress, J. Phys. Soc. Jpn. **49**, A737 (1980).
[8]A. Bussmann-Holder, G. Benedek, H. Bilz, and B. Mokross, J. Phys. (Paris) Colloq. **6**, C6-409 (1981).
[9]T. Mitsui, I. Tatsuzaki, and E. Nakamura, *An Introduction to the Physics of Ferroelectrics* (Gordon and Breach, New York, 1976).
[10]W. M. Fridkin, *Photoferroelectrics,* (Springer, Berlin, 1980).
[11]A. Bussmann-Holder, H. Bilz, and P. Vogl, *Electronic and Dynamical Properties of IV - VI Compounds,* Vol. 99 of *Springer Tracts in Modern Physics,* edited by G. Höhler, (Springer, Berlin, 1983).
[12]T. Mitsui, M. Arake, and E. Sanaguchi, in *Ferro- and Antiferroelectric Substances,* Vol. 9 of *Landolt-Börnstein,* edited by K. H. Hellwege and A. M. Hellwege (Springer-Verlag, Berlin, 1975).
[13]H. Bilz and W. Klemm, in *Raumchemie d. festen Stoffe* (Verlag L. Voss, Leipzig, 1934).
[14]G. R. Tessmann, A. H. Kohn, and W. Shockley, Phys. Rev. **92**, 890 (1953).
[15]W. Kirsch, A. Gerard, and M. Wautelet, J. Phys. C **7**, 3633 (1974).
[16]R. E. Watson, Phys. Rev. **111**, 1108 (1958).
[17]G. Thorhallson, C. Fisk, and S. Fraga, Theor. Chem. Acta. **10**, 388 (1968).
[18]A. Bussmann-Holder, H. Bilz, R. Roenspiess, and K. Schwarz, Ferroelectrics **25**, 343 (1980).
[19]R. F. Prat, Phys. Rev. A **6**, 1735 (1972).
[20]A. F. Wells, *Structural Data in Organic Chemistry,* 4th ed. (Clarendon, Oxford, 1975).
[21]W. Cochran, Adv. Phys. **9**, 387 (1960).
[22]R. A. Cowley, Philos. Mag. **11**, 673 (1965).
[23]W. G. Stirling, J. Phys. C **5**, 2711 (1972).
[24]R. Migoni, Ph.D. thesis, Stuttgart (1976).
[25]R. Migoni, R. Currat, C. H. Perry, H. Buhay, W. G. Stirling, and J. D. Axe (unpublished).
[26]H. Bilz, H. Büttner, A. Bussmann-Holder, and P. Vogl, Ferroelectrics Bull. **1**, 8 (1986).
[27]G. Kugel, M. Fontana, and W. Kress, Phys. Rev. B **39**, 813 (1987).
[28]G. Kugel, H. Vogt, W. Kress, and D. Rytz, Phys. Rev. B **30**, 985 (1984).
[29]R. Currat, R. Migoni, H. Buhay, C. H. Perrym, J. D. Axe, W. G. Stirling, and R. P. Lowndes (unpublished).
[30]G. Benedek, A. Bussmann-Holder, and H. Bilz (unpublished).
[31]R. Comes and G. Shirane, Phys. Rev. B **5**, 1886 (1972).
[32]Y. Yamada and G. Shirane, J. Phys. Soc. Jpn. **26**, 366 (1969).
[33]R. Migoni, H. Bilz, A. Bussmann-Holder, and W. Kress, *Proceedings of the International Conference on Phonon Physics, Budapest (1985),* edited by J. Kollár, N. Kroó, N. Menyhárd, and T. Siklós (World Scientific, Singapore, 1985), p. 272.
[34]D. Schmeltzer, Phys. Rev. B **28**, 459 (1983).